25th ABCM International Congress of Mechanical Engineering
October 20-25, 2019, Uberlândia, MG, Brazil

COB-2019-0443
REYNOLDS-AVERAGED NAVIER-STOKES MODELLING OF A TURBULENT LEAN PREMIXED COMBUSTOR

Alain P. N. Coimbra
Luís Fernando Figueira da Silva
Pontifícia Universidade Católica do Rio de Janeiro - Departamento de Engenharia Mecânica
R. Marquês de São Vicente, 225 - 22451-900 - Gávea, Rio de Janeiro - RJ, Brazil
coimbraalain@gmail.com

Abstract. *Lean premixed turbulent swirling flames are found in many engineering systems, such as gas turbines and jet engines. This work aims to numerically study a flame, representative of such systems, stabilized in a laboratory scale burner which uses a radial swirler. Using Reynolds-Averaged Navier-Stokes transport equations, coupled with a premixed combustion model for methane/air mixtures, a stable combustion regime is analysed in an existing combustion chamber. The flow structure is characterized here in terms of velocity fields, turbulence and combustion properties. A combustion parameter comparison is also performed, using previously obtained experimental results, yielding qualitatively similar results.*

Keywords: *Reynolds-Averaged Navier-Stokes (RANS), Premixed combustion, Swirl-stabilised combustor*

1. INTRODUCTION

Gas turbines and jet engines combustion systems of have traditionally employed diffusion flames, due to their reliability and reasonable stability characteristics (Lefebvre, 1995). However, due to increasing severe environmental restrictions regarding emissions of greenhouse gases, nitrogen oxides and soot, alternative flame configurations have been a subject of continuous research (Huang and Yang, 2009). Lean premixed turbulent flames are one of the most promising configurations, as emissions are greatly reduced due to their lower burning temperatures.

Intense studies of lean premixed flames have thus been conducted during the past few decades. These flames present multiple topologies, and are often affected by instabilities that arise from interactions between pressure fluctuations and combustion heat release oscillations (Candel *et al.*, 2014). Such instabilities may present destructive capabilities, and could be lethal in cases of aircraft engines malfunction (Goy *et al.*, 2005). It is, therefore, imperative to understand parameters that control such occurrences.

In this study, turbulent flames are modelled in a swirling flow, confined in a square-sectioned combustion chamber. This work is the modelling counterpart to the experimental studies performed at PUC-Rio. Indeed, Figueira da Silva *et al.* (2017), Piton *et al.* (2018) and Nobrega *et al.* (2019) identified and categorized different flame macro structures as a function of the swirl number. A literature review indicates that similar configurations have recently been addressed by several authors. Indeed, Shanbhogue *et al.* (2015) observed different combustion regimes and instability characteristics in turbulent methane/hydrogen flames in a swirling flow. The critical equivalence ratio for flame topology transitions was shown to change as hydrogen was added to a methane/air mixture. Transitions between topologies and their interactions with the combustion chamber walls have also been discussed by Guiberti *et al.* (2015), as parameters controlling the shape of swirl flames were identified.

Most recent numerical studies of turbulent, swirling flame dynamics employ large eddy simulations (LES). LES is a particularly attractive approach for the study of unstable regimes, where the flow field of concern is unsteady and dominated by turbulence motions that cannot be adequately resolved using classical Reynolds-Averaged Navier-Stokes models (RANS). For instance, on a turbulent premixed flame at a VOLVO rig, Rochette *et al.* (2018) studied the influence of an analytically reduced chemistry with 22 independent species, the use of a dynamic thickened flame model and a higher–order Taylor–Galerkin scheme on the quality of LES results. Lourier *et al.* (2017) examined, in a partially premixed configuration, thermoacoustic instabilities using scale adaptive simulation technique. Using two different combustion models –Eddy Dissipation Model and detailed finite rate chemistry –results investigated the mixing of fuel and air in the swirler and burner nozzle that leads to oscillations. Local and global dynamic wrinkling factors have been combined with a thickened flame model by Volpiani *et al.* (2017), in order to capture the self-excited modes of the pulsating flame in a premixed burner. Kraus *et al.* (2018) discussed the potential of coupling LES with heat transfer simulations in the burner solid structure for predicting combustion instabilities.

Despite the advances in Large Eddy Simulations, RANS models still receive attention due to their reasonable computational cost and robustness, especially in industrial processes simulations. For turbulent combustion modelling, PDF methods that treat complex, finite-rate chemistry have often been applied (Scott Brewster *et al.*, 1999). A RANS approach has also been used to investigate the swirl effects on the flame dynamics of a lean premixed combustor. Indeed, using a finite rate eddy-dissipation model with a three-step global reaction mechanism, flame stability limits have been defined, and flow behaviour and flame dynamics have been described (Mansouri *et al.*, 2016). The Realizable $k-\epsilon$ model has been pointed out as the most predictive for high swirl numbers, as it has shown best agreement with experimental results.

Several experimental studies have been conducted in order to better understand thermoacoustic instabilities also. Using OH–PLIF, Schulz *et al.* (2018) studied interactions between acoustic pressure and heat release fluctuations in unstable operating conditions of a sequential combustor. Chemiluminescence and dynamic pressure measurements allowed Noh *et al.* (2018) to study thermoacoustic instabilities in a cylindrical combustion chamber. Additionally, through the use of dynamic mode decomposition, the azimuthal transport of hot combustion products around the centerline of the combustion chamber could be analyzed. Han *et al.* (2018) identified three common flame macrostructures and their respective instabilities in stratified swirling flames as a function of equivalence ratio and stratification ratio.

The objective of the present work is to model, using a RANS approach, the lean premixed turbulent swirling combustor developed at PUC-Rio in partership with Centrale Supelec EM2C laboratory. The results of such a model are expected to shed light on the flow field structures observed in the steady operating regimes of this combustor. Reactive flow simulations are performed, in order to identify and characterize the studied flame topology.

2. NUMERICAL METHODOLOGY

2.1 COMPUTATIONAL DOMAIN

The configuration of interest consists of a radial swirler and the adjoining combustion chamber. The swirler is a mechanical device that induces a significant amount of angular momentum to the flow, and its overall design, inlet and outlet sections are presented in Fig. 1. The methane/air mixture is introduced in the swirler through six orifices, radially distributed at its base. The internal cylindrical structure induces an annular flow inside the device. The bluff body is an inverted conical structure flushed to the top of the swirler exit surface, and its main function is to provide for the flame anchoring near the combustion chamber base.

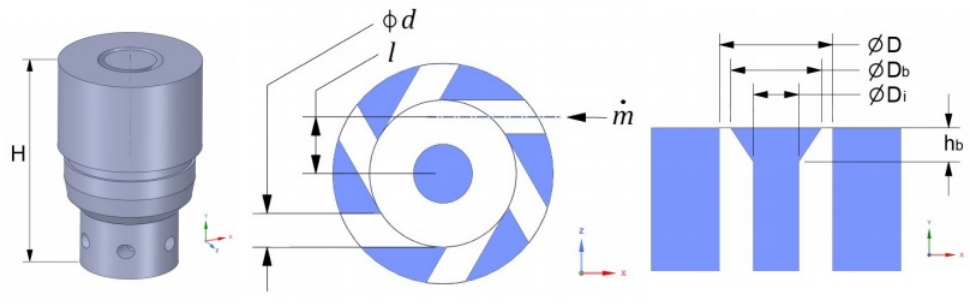

Figure 1. Swirler (left) and swirler inlet section (middle) and exit section (right).

The swirl number is an important parameter for characterizing the intensity of the swirling motion. It is defined by the ratio between the axial flux of tangential momentum, G_θ, and the axial momentum flux, G_z (Durox *et al.*, 2013):

$$S = \frac{G_\theta}{RG_z} = \frac{\int_0^R u_z u_\theta r^2 dr}{R\int_0^R u_z^2\, r dr}, \tag{1}$$

where R is the swirler radius. The swirl number has been estimated from its geometrical properties, assuming a solid body rotation flow within the device, a uniform axial velocity and negligible pressure effects (Nobrega *et al.*, 2019). The corresponding geometrical swirl number is thus written as:

$$S = \frac{lD}{nd^2}\left[1-\left(\frac{D_b}{D}\right)^2\right] \approx 0.4, \tag{2}$$

where l is the offset distance of the inlet orifice, relative to the main axis, D is the swirler outer diameter, n is the number of orifices, d is the orifice diameter, and D_b is the diameter of the inverted cone base. For the studied swirler, $l = 3.85$ mm, $D = 10$ mm, $n = 6$, $d = 2.3$ mm and $D_b = 8$ mm.

The combustion chamber, represented in Fig. 2, is square-sectioned, with a width of $L = 40$ mm. The actual chamber height in the experimental setup is $H_c = 170$ mm, but it has been adapted to $H_c = 100$ mm in this work due to limitations in the available computational resources. As a consequence, regimes with long flames are expected to present discrepancies with respect to the experimental data, as it will be discussed in the next section. A pyramid-shaped convergent structure is placed at the top of the combustion chamber, which provokes a flow acceleration at the domain outlet. The top structure has a height of $H_p = 15$ mm and the outlet has a width of $L_p = 10$ mm. This structure is a modelling artefact which also diverges from the experimental counterpart of this work. Indeed, the acceleration of the flow near the domain outlet has proved to prevent the occurrence of reverse flow, which interferes with the converging process of the numerical solution.

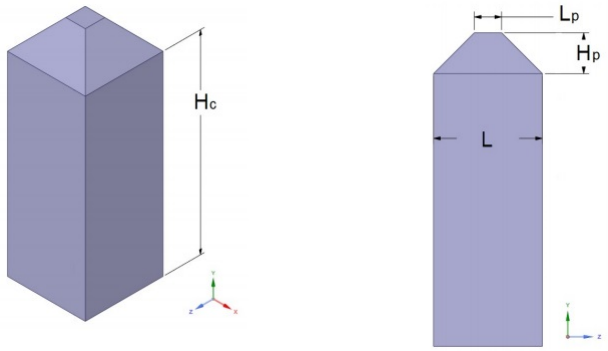

Figure 2. Combustion chamber isometric view (left) and frontal view (right).

2.2 NUMERICAL MODEL DESCRIPTION

The numerical simulations in this work have been performed using the Fluent code (Ansys). This is motivated by a partnership with Ansys/France in the framework of the Magister consortium (Consortium, 2019). The physical and chemical models used here are directly chosen from this code available choices.

In all studied cases, the balance equations of momentum and pressure have been solved, together with turbulence and combustion models. The functions and particularities of each model are briefly discussed and their primary sources are referenced, where they have been derived and presented with a more detailed description. First, the turbulence model of choice is examined, which has been applied to isothermal and reactive flow studies. The premixed combustion model is then addressed. Finally, the method for defining premixed flame properties is exposed.

2.2.1 Turbulence: Realizable $k-\epsilon$ model

The $k-\epsilon$ model is a widely used turbulence model and it is found in most commercial CFD codes. It is often described as a robust, economic and reasonably accurate solution for a wide range of industrial flows and heat transfer simulations (Fluent, 2019). Its first transported property is the turbulent kinetic energy k, which describes the energy of the turbulent fluid motion. The second one is commonly referred to as the turbulent dissipation, ϵ, which determines the small scales of the turbulence. The third important specification in the $k-\epsilon$ model is the turbulent viscosity, which is modelled as a function of these transported flow properties using the Boussinesq hypothesis (Jones and Launer, 1972). In the derivation of the $k-\epsilon$ model, it is assumed that the flow is fully turbulent (corrections for flows with low Reynolds-numbers are therefore required) and the effects of molecular viscosity are negligible.

The realizable $k-\epsilon$ is a more recent model which consists mainly of a different formulation for the turbulent viscosity (Shih *et al.*, 1995). The standard two-equation model is known to be over-predictive for the eddy viscosity in cases of flows with a high mean shear rate, due to its turbulent viscosity formulation. This formulation is thus improved by insuring mathematical realizability, involving the effect of mean rotation on turbulence stresses, and avoiding negative normal stresses in cases of large mean strain rates. This model also incorporates a new dissipation rate equation, based on the dynamic equation for fluctuating vorticity. It has been shown to predict more accurately the behaviour of flows involving rotation (Shih *et al.*, 1995).

2.2.2 Premixed combustion: Extended Coherent Flamelet Model

The combustor studied in this work belongs to the group of premixed combustion devices. A perfectly homogeneous methane and air mixture is assumed to enter the domain, with a known fuel/air equivalence ratio. A two-equation choice of classical premixed combustion model is considered in this work: the Extended Coherent Flamelet Model (ECFM)

(Poinsot and Veynante, 2005).

The first transport equation of the ECFM accounts directly for the turbulent premixed combustion: the reaction progress variable, c. In this formulation, a one-step, irreversible chemical reaction between fresh gases and combustion products is considered. The progress variable c is a binary entity, where $c = 0$ denotes fresh gases and $c = 1$ denotes burnt gases. This variable has been introduced, and its consequences to modelling analysed by Bray, Moss and Libby (Bray *et al.*, 1985). The progress variable is usually interpreted as a normalized temperature:

$$c = \frac{T - T_u}{T_b - T_u}, \tag{3}$$

where T_u and T_b denote the unburnt and burnt temperatures, respectively.

The usual additional assumptions for the numerical model formulation simplification are: perfect gases, incompressible flow, constant heat capacities and unity Lewis numbers. This model also assumes that the flame time scale is smaller than the smallest turbulence time scales, also known as the Kolmogorov eddies. As a consequence, the effect of turbulence is to wrinkle the flame sheet (Borghi and Champion, 2000). The chemical reaction and the internal flame structure should remain unaltered from the laminar case.

The unclosed transport equation of the averaged progress variable, $\tilde{c}$, has the form:

$$\frac{\partial}{\partial t}\left(\bar{\rho}\tilde{c}\right) + \frac{\partial}{\partial x_i}\left(\bar{\rho}\tilde{u_i}\tilde{c}\right) = \frac{\partial}{\partial x_i}\left(\bar{\rho}\,\frac{\nu_t}{Sc_c}\frac{\partial \tilde{c}}{\partial x_i}\right) + \bar{\dot{w}}_c. \tag{4}$$

Both time-based (Reynolds) and density-based (Favre) averages have classically been used, denoted as $(\bar{\cdots})$ and $(\tilde{\cdots})$, respectively (Pope, 2000). The first term on the RHS of the equation is a closure of turbulent scalar fluxes, often known as the gradient assumption, and it is often used in turbulent combustion models (Darabiha *et al.*, 1989). The turbulent viscosity ν_t is estimated from the turbulence model, as discussed in the previous section. The turbulent Schmidt number is defined as the ratio of the turbulent transport of momentum and the turbulent transport of mass and it is assumed to have a constant value of $Sc_c = 0.7$.

The average chemical source term, $\bar{\dot{w}_c}$, is determined from the flame surface density, Σ, which accounts for the turbulence/combustion interaction (Poinsot and Veynante, 2005). This mean reaction rate is then modelled as:

$$\bar{\dot{w}_c} = \rho_u U_l \Sigma, \tag{5}$$

where ρ_u denotes the density of the unburnt gases and U_l, the flame speed, is an intrinsic property of premixed combustible mixtures.

The equation for the transport of the net flame area per unit volume, Σ, may be written as:

$$\frac{\partial}{\partial t}\left(\Sigma\right) + \frac{\partial}{\partial x_i}\left(\tilde{u_i}\Sigma\right) = \frac{\partial}{\partial x_i}\left(\frac{\nu_t}{Sc_c}\frac{\partial \Sigma}{\partial x_i}\right) + \kappa_t\Sigma - D, \tag{6}$$

where κ_t and D are unclosed terms which require, therefore, modelling. The turbulent strain rate, κ_t, is related to the stretch rate of the flame due to the turbulence motions, and D is a destruction term required to avoid the infinite growth of the flame surface area (Candel and Poinsot, 1990).

The turbulent strain rate is estimated by the Intermittent Turbulent Net Flame Stretch (ITNFS) technique as a function of a turbulent time scale ϵ/k and an efficiency parameter Γ_K, which is a function of flame/turbulence interaction quantities and is fitted from DNS data (Meneveau and Poinsot, 1991):

$$\kappa_t = \alpha_0\,\Gamma_K\left(\frac{u'}{U_l}, \frac{l_t}{\delta_l}\right)\frac{\epsilon}{k}, \tag{7}$$

where α_0 is a constant, $\alpha_0 = 1.6$, u' is the root-mean-square velocity fluctuation, l_t is the integral turbulence length scale and δ_t is the laminar flame thickness.

The flame area destruction term is modelled in this work as:

$$D = \beta\,U_l\,\frac{\Sigma^2}{1-c}, \tag{8}$$

where β is a constant with the value of one.

The adiabatic combustion temperature, T_b, and laminar flame speed, U_l, for methane/air combustion, have been determined as a function of the equivalence ratio $\phi \in [0.4, 1.0]$ at atmospheric conditions. A good agreement has been obtained with experimental results for the laminar flame speed (Coppens *et al.*, 2007). These numerical simulations have been carried out with the CHEMKINPRO code, using the GRIMECH 3.0 mechanism for kinetics, thermodynamics and transport properties of the involved species (Smith *et al.*, 1999). This classical mechanism consists of 53 species and 325 reactions. For the adiabatic flame temperature and laminar flame speeds, the equilibrium and premixed flame speed models have been used, respectively. The obtained values of T_b are used in Eq.(3), and values of U_l are used for a metric in the combustion/turbulence interaction study and for the calculation of the mean reaction rate, determined with Eq.(5).

2.2.3 Mesh generation and boundary conditions

The computational grid has been obtained in this work using the software *Fluent Meshing* from *Ansys*. A three-dimensional mesh is generated from the computational domain described in the previous section. The meshing in this work consists of unstructured polyhedral elements.

The meshing is refined at the swirler's surface and lower combustion chamber regions, where larger gradients of velocity, turbulence and combustion properties are expected to occur. Only one element is placed normal to the wall surfaces throughout the domain, with a length of $\Delta = 0.035$ mm on the smallest cells, which are located around the inverted cone base. The average cell size in the swirler region, around the swirler exit surface, in the lower part of the combustion chamber and in the top part of the combustion chamber are $\Delta = 0.30$, $\Delta = 0.10$, $\Delta = 0.23$ and $\Delta = 1.00$ mm, respectively.

The six inlets at the base of the swirler are set as pressure inlet boundary conditions (BC). A fixed absolute pressure of $P_{in} = 101$ kPa is set in all inlet surfaces, illustrated in Fig. 1. The outlet is the reduced area at the top of the combustion chamber, resulted from the inclusion of the pyramid-shaped structure, depicted in Fig. 2. This area has been designed to equal the total surface area of the six inlet surfaces, which is a technique for preventing the occurrence of reverse flow at the outlet boundaries. A constant mass flow rate BC is set at the outlet surface, directed outwards, relative to the computational domain. All walls have no slip and adiabatic conditions, i.e., zero heat exchange with the exterior.

3. RESULTS AND DISCUSSION

The reactive flow study performed in this section has been carried out with the realizable $k-\epsilon$ turbulence model, coupled with the two-equation extended coherent flamelet premixed combustion model, described in the previous section. The fluid mixture properties are $\rho = 1.225$ kg/m^3 and $\mu = 1.79$ kg/m·s for density and dynamic viscosity, respectively. The flame regime treated in this work is known as Flame IV, as defined and characterized experimentally by Shanbhogue *et al.* (2015), Piton *et al.* (2018) and Nobrega *et al.* (2019). In order to numerically obtain this flame topology, a methane/air equivalence ratio of $\phi = 0.8$ is used, for which the values of adiabatic combustion temperature and laminar flame velocity are $T_b = 1996$ K and $U_l = 27.8$ m/s, respectively. The total mass flow rate through the six combined inlet orifices is $\dot{m} = 0.001715$ kg/s, which corresponds to a volumetric flow rate of $\dot{\forall} = 1400$ cm^3/s, chosen to represent the higher values experimentally studied. Boundary conditions follow the procedure described in the preceding section. The pressure-based coupled algorithm is used for pressure-velocity coupling.

3.1 OVERALL FLOW STRUCTURE

A general scheme of the computational domain is given by Fig. 3. As it may be seen, the superimposed pathlines indicate the flow motion within the domain. As the orifices are offset with respect to the swirler main body axis, a significant amount of tangential momentum is induced inside the annular region of the swirler body. The fluid flows upwards inside the swirler, between the external wall and an internal cylindrical structure. The bluff body narrows the flow path section, before the mixture finally expands as it flows upwards at the swirler exit and into the combustion chamber. Due to the sudden expansion, an external recirculation may also be seen at the corners of the chamber, represented by a flow redirection towards the square combustor base.

In order to allow for a more detailed analysis, the flow field within the combustion chamber is now studied. The swirling jet expansion and recirculation is represented in Fig. 4, through contours of the vertical velocity component, v_y, at heights $y = 0, 10, 20, 30$ and 40 mm, from the combustion chamber base. A good 45° symmetry may be observed, i.e., with respect to the four corners of the combustion chamber. As it may be seen from the regions of high velocity in the positive direction of the y axis, the jet expands from the swirler exit and interacts with the chamber walls, at a height between $y = 10$ mm and $y = 20$ mm. An outer recirculation zone (ORZ) can be seen at the four corners of the chamber beneath this height, represented by a flow redirection towards the base. Both the expansion and swirling motion also generate a pressure deficit at the center of the computational domain, not shown here for the sake of brevity, which causes an inner recirculation zone (IRZ), represented by a flow redirection towards the swirler buff-body also.

The swirl number has also been determined numerically by Eq.(1), as the ratio between the axial flux of tangential momentum and the axial momentum flux through the swirler exit surface, which is represented in Fig. 1. The obtained value is $S = 0.81$, which is significantly higher that the geometrical approximation of $S = 0.4$. It may be inferred that the assumptions on the geometrical approximation from Eq.(2) could over-simplify the flow properties. This is currently under investigation, and will be subject of future work.

Further analysis of the flow field, turbulence and combustion properties is possible by analysis of the results illustrated in Fig. 5. The depicted section is perpendicular to the combustion chamber base and lateral windows and crosses the swirler at the center of the bluff-body, thus allowing to visualize the lower part of the combustion chamber from the swirler exit surface. Figure 5(a) and (b) depict the velocity field in the vertical and horizontal directions, i.e., v_y and v_x. It may be observed, in greater detail than in Fig. 4, the expansion of the swirling jet from the swirler exit to the chamber

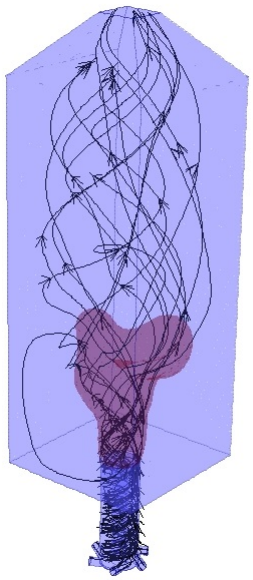

Figure 3. Schematic view of the computational domain (blue) with superimposeed pathlines (black). The anchored flame surface is also displayed (red), represented by a progress variable iso-surface $c = 0.5$. A stoichiometric mixture is used in this scheme.

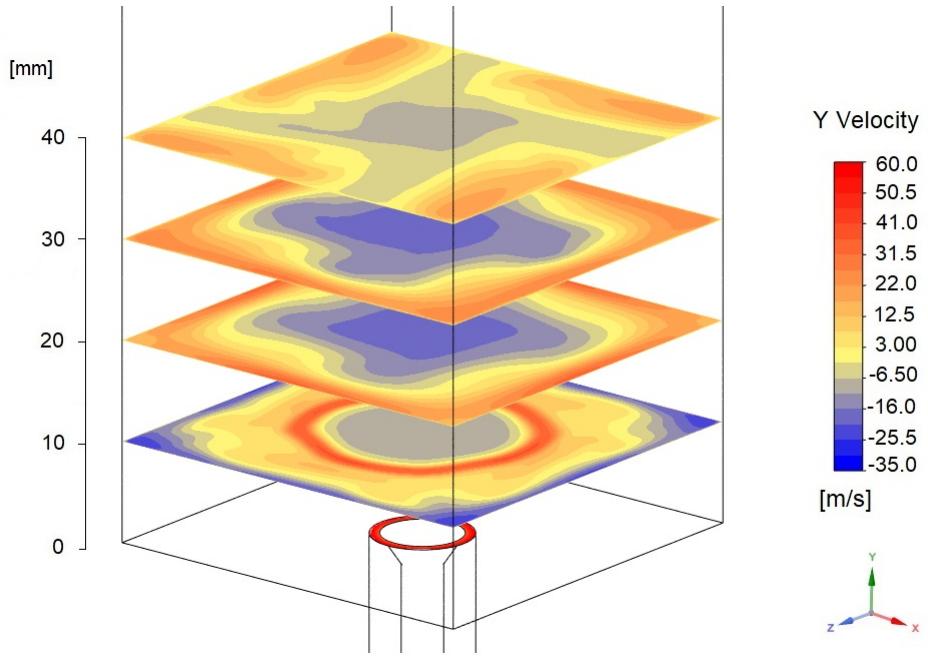

Figure 4. Contours of vertical velocity for heights $y = 0,\ 10,\ 20,\ 30$ and 40 mm, from the combustion chamber base, for a methane/air equivalence ratio $\phi = 0.8$ and volumetric flow rate $\dot{\forall} = 1400$ cm^3/s.

walls. The inner and outer recirculation zones may be perceived also, from the flow redirection towards the combustor bottom. Figure 5(c) gives the temperature field at the outer recirculation zone. As it may be seen, a recirculation of hot gases, at $T \approx 1300K$, occurs in this region, which is the main characteristic of this flame regime (Shanbhogue *et al.*, 2015). From Figs. 5(a) and (c), a flow of high velocity magnitude of hot gases adjacent to the chamber walls may be identified. It could be inferred that the used assumption of zero heat flux at the walls in the boundary conditions may lead to an under-prediction of the heat flux in the system and, therefore, to an incorrect temperature distribution. Figure 5(d) depicts the turbulent viscosity ratio, with an emphasis at the ORZ and swirling jet regions. This non-dimensional property is the ratio between the turbulent viscosity μ_t and the molecular dynamic viscosity μ. The values of this property

suggest that the flow turbulence in the ORZ is $\mu_t/\mu \approx 10$, which represents a significant turbulence level. The Damköhler number compares an integral turbulence time scale to a characteristic chemical time scale of the heat release process. From Fig. 5(e), it may be seen that the values of Da are significantly low ($Da < 1$) in the swirling jet upstream to the flame. This indicates that, according to this Da estimation, this flame could be situated in the thickened flamelet regime in the Borghi diagram (Borghi and Champion, 2000), which would not be suited for the coherent flame model applied here. Note that this Da estimate is based on an order of magnitude analysis of the thermal flame thickness, which could differ from the value computed using detailed chemistry and transport by an order of magnitude (Grosseuvres *et al.*, 2019). These issues are currently under scrutiny and will be fully addressed in future works. Figure 5(f) depicts the distribution of the flame area density, Σ, computed by solving Eq.(6), which indicates that the flame surface lies around the fuel/air swirling jet and, again, exhibits a strong interaction with the wall.

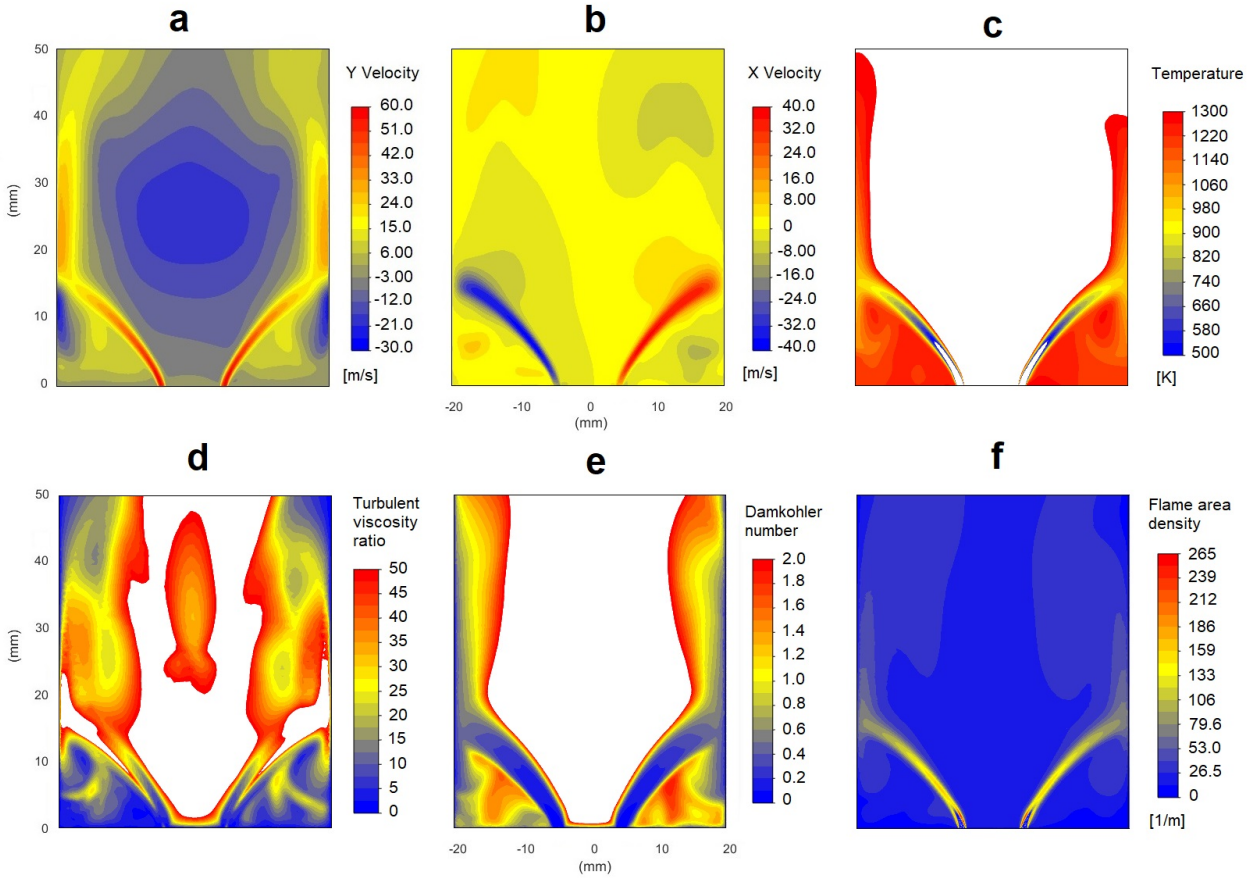

Figure 5. Contours of flow and combustion properties. (a): vertical velocity; (b): horizontal velocity; (c): temperature field at the ORZ; (d): turbulent viscosity ratio at the swirling jet and ORZ; (e): Damköhler number at the swirling jet and ORZ; (f): flame area density (Σ).

3.2 COMPARISON WITH EXPERIMENTAL RESULTS

In order to gain further insight of the flow field, a comparison between numerical and experimental results for a representation of the average flame brush may be seen in Fig. 5. The experimental instantaneous PLIF-OH signal has been binarized, assuming a zero value when OH is absent, and one when OH is present (Nobrega *et al.*, 2019). As a consequence, the binarized results could represent a progress variable, where $c = 0$ denotes fresh gases and $c = 1$ denotes burnt gases, obtained from Eq.(4). The average value of this property should then represent the mean flame surface. For this studied flame, the topology is that of an outer recirculation zone flame (Shanbhogue *et al.*, 2015), where the flame surface stabilizes around the expanding jet, ORZ and chamber walls. As it can be seen from Fig. 5, the computed progress variable field predicts the average flame around the expanding jet and outer recirculation zones. In the ORZ, the mean progress variable value is $c \approx 0.5$, and downstream to the swirling jet $c \approx 0.8$. The flame expands and stars to interact with the combustion chamber walls at similar positions, $y \approx 15$ mm, from the chamber base. The agreement between the model and the experiments is qualitative. In particular, the average flame brush thickness obtained experimentally may be seen to be larger than the computed counterpart. Nevertheless, the overall position of this flame front is adequately

predicted. The obtained discrepancies could be due to the above mentioned model shortcomings, which will be subject of future works.

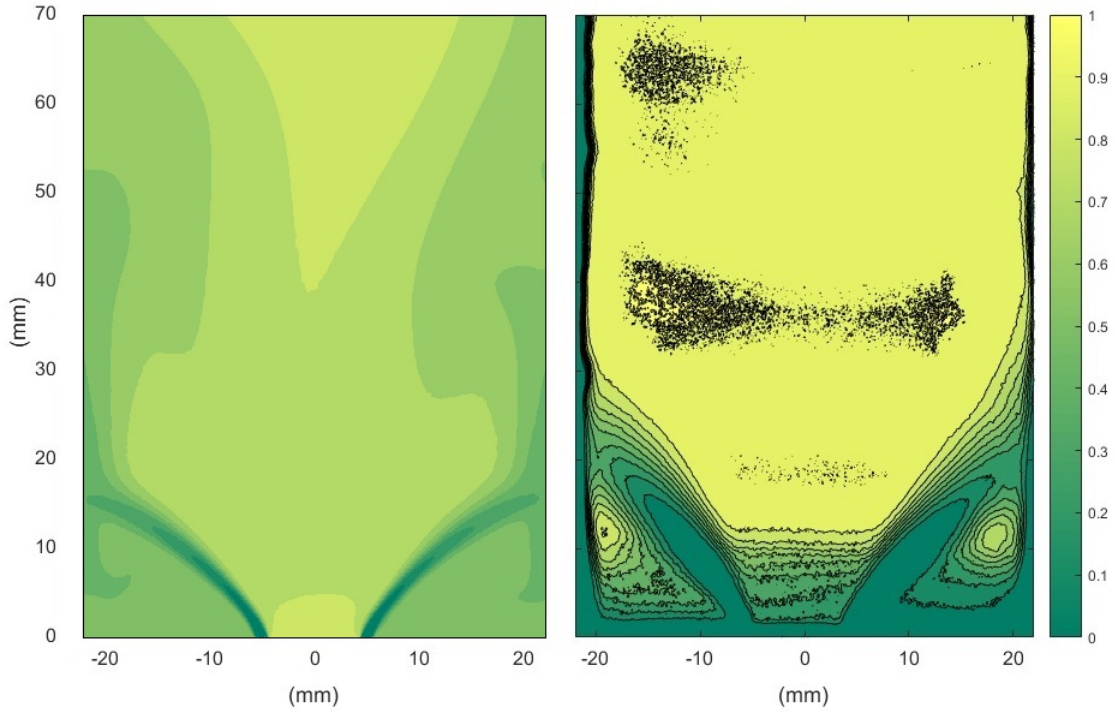

Figure 6. Flame regime IV: contours of computed progress variable (left) and average OH radical binarized image, measured with PLIF (right), adapted from Nobrega *et al.* (2019).

4. ACKNOWLEDGEMENTS

This study was financed in part by the Coordenação de Aperfeiçoamento de Pessoal de Nível Superior - Brasil (CAPES) - Finance Code 001 (Alain P. N. Coimbra). This work was performed while L. F. Figueira da Silva was on leave from Institut Pprime (CNRS, France). The authors gratefully acknowledge the support for the present research provided by Conselho Nacional de Desenvolvimento Científico e Tecnológico (CNPq, Brazil) under research grants no. 403904/2016-1. The authors are also grateful to Dr. Valéry Morgenthaler (Ansys/France) for the assistance and helpful comments on this work.

5. REFERENCES

Borghi, R. and Champion, M., 2000. *Modélisation et théorie des flammes*. Editions TECHNIP, 1st edition.

Bray, K.N.C., Libby, P.A. and Moss, J.B., 1985. "Unified modeling approach for premixed turbulent combustion – part I: General formulation". *Combustion and Flame*, Vol. 61, pp. 87–102.

Candel, S., Durox, D., Schuller, T., Bourgouin, J.F. and Moeck, J.P., 2014. "Dynamics of swirling flames". *Annual Review of Fluid Mechanics*, Vol. 46, pp. 147–173.

Candel, S.M. and Poinsot, T.J., 1990. "Flame stretch and the balance equation for the flame area". *Combustion Science and Technology*, Vol. 70, pp. 1–15.

Consortium, M., 2019. "Magister consortium". https://www.utwente.nl/en/et/magister/AboutMagister/Consortium/.

Coppens, F.H.V., De Ruyck, J. and Konnov, A.A., 2007. "Effect of hydrogen enrichment on adiabatic burning velocity and NO formation in methane + air flames". *Experimental Thermal and Fluid Science*, Vol. 31, pp. 437–444.

Darabiha, N., Giovangigli, V., Trouvé, A., Candel, S.M. and Esposito, E., 1989. "Coherent flame description of turbulent premixed ducted flames". *Turbulent Reactive Flows*, Vol. 40, pp. 591–637.

Durox, D., Moeck, J.P., Bourgouin, J.F., Morenton, P., Viallon, M., Schuller, T. and Candel, D., 2013. "Flame dynamics of a variable swirl number system and instability control". *Combustion and Flame*, Vol. 160, pp. 1729–1742.

Figueira da Silva, L.F., Mergulhão, C.S., Piton, L., Scouflaire, P. and Darabiha, N., 2017. "Experimental study of a lean premixed turbulent swirling flame stabilization". *24th International Congress of Mechanical Engineering*, pp. 1–9.

Fluent, I., 2019. "Standard, RNG, and realizable k-ϵ models theory". https://www.sharcnet.ca/Software/Fluent6/html/ug/node477.htm.

Goy, C.J., James, S.R. and Rea, S., 2005. "Combustion instabilities in gas turbine engines: operational experience, fundamental mechanisms, and modeling". *Journal of Engineering for Gas Turbines and Power*, Vol. 210, pp. 163–175.

Grosseuvres, R., Comandini, A. and Chaumeix, A.B.N., 2019. "Combustion properties of H_2/N_2/O_2/steam mixtures". *Proceedings of the Combustion Institute*, Vol. 37, pp. 1537–1546.

Guiberti, T.F., Durox, D., Zimmer, L. and Schuller, T., 2015. "Analysis of topology transitions of swirl flames interacting with the combustor side wall". *Combustion and Flame*, Vol. 162, pp. 1–16.

Han, X., Laera, D., Morgans, A.S., Sung, C.J., Hui, X. and Lin, Y.Z., 2018. "Flame macrostructures and thermoacoustic instabilities in stratified swirling flames". *Proceedings of the Combustion Institute*, Vol. 37, pp. 1–8.

Huang, Y. and Yang, V., 2009. "Dynamics and stability of lean-premixed swirl-stabilized combustion". *Progress in Energy and Combustion Science*, Vol. 35, pp. 293–364.

Jones, W.P. and Launer, B.E., 1972. "The prediction of laminarization with a two-equation model of turbulence". *International Journal of Heat and Mass Transfer*, Vol. 15, pp. 301–314.

Kraus, C., Selle, L. and Poinsot, T., 2018. "Coupling heat transfer and large eddy simulation for combustion instability prediction in a swirl burner". *Combustion and Flame*, Vol. 191, pp. 1–13.

Lefebvre, A.H., 1995. "The role of fuel preparation in low-emission combustion". *Journal of Engineering for Gas Turbines and Power*, Vol. 117, pp. 617–654.

Lourier, J.M., Stöhr, M., Noll, B., Werner, S. and Fiolitakis, A., 2017. "Scale adaptive simulation of a thermoacoustic instability in a partially premixed lean swirl combustor". *Combustion and Flame*, Vol. 183, No. 1, pp. 1–15.

Mansouri, Z., Aouissi, M. and Boushaki, T., 2016. "A numerical study of swirl effects on the flow and flame dynamics in a lean premixed combustor". *International journal of heat and Technology*, Vol. 34, pp. 227–235.

Meneveau, C. and Poinsot, T., 1991. "Stretching and quenching of flamelets in premixed turbulent combustion". *Combustion and Flame*, Vol. 86, pp. 311–332.

Nobrega, G.S., Piton, L.C., Figueira da Silva, L.F. and Darabiha, P.S.N., 2019. "Experimental study of the effect of the swirl number on premixed combustion regimes and flame topologies". *11th Mediterranean Combustion Symposium*, pp. 1–12.

Noh, D., Karlis, E., Navarro-Martinez, S., Hardalupas, Y., Taylor, A.M.K.P., Fredrich, D. and Jones, W.P., 2018. "Azimuthally-driven subharmonic thermoacoustic instabilities in a swirl-stabilised combustor". *Proceedings of the Combustion Institute*, Vol. 37, pp. 1–9.

Piton, L., Nobrega, G.S., Figueira da Silva, L.F., Scouflaire, P. and Darabiha, N., 2018. "Experimental study of the influence of the swirl number on lean premixes combustion regimes". *17th Brazilian Congress of Thermal Sciences and Engineering*, pp. 1–9.

Poinsot, T. and Veynante, D., 2005. *Theoretical and Numerical Combustion*. R. T. Edwards Inc., Philadelphia, PA 19118 USA, 2nd edition.

Pope, S.B., 2000. *Turbulent Flows*. University of Cambridge, Edinburgh Building, Cambridge, CB2 2RU, UK, 1st edition.

Rochette, B., Collin-Bastiani, F., Gicquel, L., Vermorel, O., Veynante, D. and Poinsot, T., 2018. "Influence of chemical schemes, numerical method and dynamic turbulent combustion modeling on LES of premixed turbulent flames". *Combustion and Flame*, Vol. 191, pp. 1–14.

Schulz, O., Doll, U., Ebi, D., andn C Bourquard, J.D. and Noiray, N., 2018. "Thermoacoustic instability in a sequential combustor - large eddy simulation and experiments". *Proceedings of the Combustion Institute*, Vol. 37, pp. 1–8.

Scott Brewster, B., Cannon, S.M., Farmer, J.R. and Meng, F., 1999. "Modelling of lean premixed combustion in stationary gas turbines". *Progress in Energy and Combustion Science*, Vol. 25, pp. 353–385.

Shanbhogue, S.J., Sanusi, Y.S., Taamallah, S., Habib, M.A. and Mokheimer, E.M.A., 2015. "Flame macrostructures, combustion instability and extinction strain scaling in swirl-stabilized premixed CH4/H2 combustion". *Combustion and Flame*, Vol. 163, pp. 1–14.

Shih, T.H., Liou, W.W., Shabbir, A., Yang, Z. and Zhu, J., 1995. "A new $k-\epsilon$ eddy viscosity model for high Reynolds number turbulent flows". *Computers Fluids*, Vol. 24, pp. 227–238.

Smith, G.P., Golden, D.M., Frenklach, M., Moriarty, N.W., Eiteneer, B., Goldenberg, M., Bowman, C.T., Hanson, R.K., Song, S., Gardiner Jr, W.C., Lissianski, V.V. and Qin, Z., 1999. "http://www.me.berkeley.edu/gri_mech/". *Berkeley Mechanical Engineering*.

Volpiani, P.S., Schmitt, T. and Veynante, D., 2017. "Large eddy simulation of a turbulent swirling premixed flame coupling the TFLES model with a dynamic wrinkling formulation". *Combustion and Flame*, Vol. 180, pp. 1–12.